Study of end effects on the performance of the linear switched reluctance motor

Garcia Amorós J.[1] , Andrada Gascón P.[2]

[1] Departament d'Enginyeria Electrònica, Eléctrica i Automàtica
E.T.S.E., Universitat Rovira i Virgili
Avinguda Països Catalans, 26, 43007 Tarragona, Spain
Tel.:+34 977 559695, fax:+34 977559605
E-mail: jordi.garcia-amoros@urv.cat

[2] **GAECE.** Grup d'Accionamients Elèctrics amb Commutació Electrònica
Departament d'Enginyeria Elèctrica, EPSEVG-UPC
Víctor Balaguer s/n, 08800 Vilanova i la Geltrú, Spain
Tel.:+34 938967732; fax: +34 938967700
E-mail: andrada@ee.upc.edu

Abstract. The purpose of this paper is to study the end effects in a double-sided linear switched reluctance motor (LSRM). Switched reluctance motors (SRM) and by extension their linear counterpart, LSRM, have been widely studied using two-dimensional finite element analysis (2D FEA). End effects are not included in 2D FEA, even though these effects considerably increase unaligned inductance. This paper describes a procedure that takes into account the end effects in flux linkage, inductance and force profiles on LSRM. It is based on 2D FEA corrected by the inclusion of end-winding inductance and several empirical coefficients. The results of this approach closely coincide with experimental measurements.

Key words

Finite element analysis, linear switched reluctance machine, end effects, analytical modelling

1. Introduction

The SRM has been widely studied using two-dimensional finite element software packages, which have proven an effective approach for analysing SRM performance. However, end effects are not included in 2D FEA even though these effects can increase unaligned inductance by up to 20-30% [1], as the shorter the machine, the higher the increase. The results of this are a reduced energy conversion area predicted by 2D FEM and, therefore, lower performance calculations. End effects appear at the end of the lamination stack and are basically the consequence of extra flux linkages produced at the head or the end of the winding. This extra flux produces an axial fringing flux that, along with the steel imaging effect of the laminations, contributes to increasing these effects [2]. Several papers have dealt with end effects in SRM [2], [3], [4], [6] and in LSRM [7]. The most accurate way to estimate end effects is probably by means of 3D FEA, but available 3D FEA software packages are expensive and require a long computation time. With the aim of estimating end effects within a reasonable computing time, some studies have combined 2D FEA and analytical methods [4], [7]. The purpose of this paper is to study end effects in a double-sided linear switched reluctance motor (LSRM). A procedure is proposed based on 2D FEM corrected by the inclusion of end-winding inductance and several empirical coefficients.

2. The End Effects Approach

A. Problem description

The main dimensions of the LSRM are shown in Fig. 1, which provides a view of only a portion of the motor. A detailed view of the head or end-winding is shown in Fig. 2.

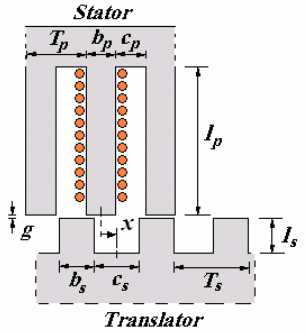

Fig. 1. Main dimensions of the LSRM

The distance between the aligned and unaligned positions (S) is calculated by:

$$S = \left(b_s + c_s\right)/2 \qquad (1)$$

Where b_s and c_s are the translator pole width and slot width. For $x = 0$ the poles are fully unaligned and for $x = S$ the poles are fully aligned (see Fig. 1).

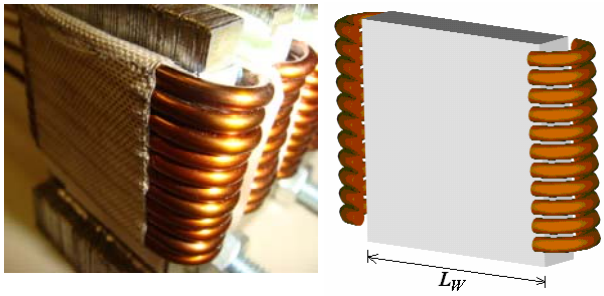

Fig. 2. 3D view of end-winding

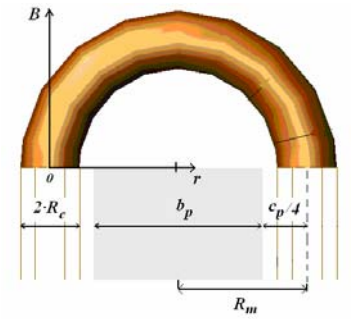

Fig. 3. Geometrical parameters for L_{end} calculation

B. End-effects coefficient

End effects in 2D FEA are taken into account by means of the end-effects coefficient, K_{ee} , [5] dependent of the current density (J) and position (x), given by:

$$\psi_{3D} = K_{ee} \cdot \psi_{2D} \tag{2}$$

$$L_{3D} = K_{ee} \cdot L_{2D} \tag{3}$$

Where Ψ_{2D} and L_{2D} are the flux linkage and the inductance obtained in 2D FEA and Ψ_{3D} and L_{3D} are the 3D flux linkage and the inductance approaches that account for the end effects and are most similar to the measured values. The correction factor K_{ee} is defined as [4]:

$$K_{ee} = \left(1 + \frac{L_{end} \cdot K_{si}}{L_{2D}}\right) \cdot K_f \tag{4}$$

Where, L_{end} is the end-winding inductance, K_{si} is a factor that affects L_{end} due to the steel imaging effect and K_f is the axial fringing factor. K_{si} can usually be omitted (K_{si} = 1) since its effect on L_{end} is generally less than 2% [4].

C. Fringing flux coefficient

The axial fringing flux is due to the tendency of the magnetic flux to bulge out in an axial direction. This effect is stronger when the poles are fully unaligned (x = 0) and weaker when the poles are completely aligned (x = S). Therefore, depending on the translator position (x), and the axial fringing factor (K_f) can be calculated by:

$$K_f(x) = \frac{L_W + l_g(x)}{L_W} \tag{5}$$

Where $l_g(x)$ is the effective air gap length and L_W is the stack length affected by the stacking factor k_{fe}. For the aligned position the effective air gap length is $l_g(0) = g$ and for the unaligned position $l_g(S)$ = g + l_s, where l_s is the translator pole length [1].
For intermediate positions ($0 < x < S$) the authors propose a new procedure in which the effective air gap length is the air gap plus the translator pole length modulated by a function $f_m(x)$, that is:

$$l_g(x) = g + l_s \cdot f_m(x) \tag{6}$$

The modulation function $f_m(x)$ has to verify: $f_m(0) = 1$ and $f_m(S) = 0$, so the following expression provides the most closely fitting results:

$$f_m(x) = \frac{1}{2} \cdot \left(1 + \cos\left(\pi \cdot x / S\right)\right) \tag{7}$$

Therefore, the axial fringing factor results:

$$K_f(x) = 1 + \frac{2 \cdot g + l_s \cdot \left(1 + \cos\left(\pi \cdot x / S\right)\right)}{2 \cdot L_W} \tag{8}$$

The end-effect coefficient is finally obtained after substituting (8) in (4). Fig. 4 shows the plot of $K_{ee}(J,x)$ for the LSRM prototype described in section 4.

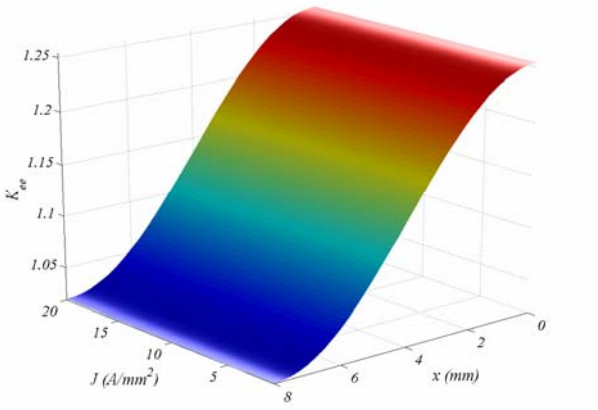

Fig. 4. Correction factor K_{ee}

3. End-Winding Inductance

End-winding inductance, $L_{end,}$ can be analytically deduced from Fig. 3 or can be computed by means of an axis-symmetrical 2D finite element model.

A. End-winding inductance: Analytical calculation

End-winding inductance can be analytically obtained by considering end winding as a straight group of wires of the same length placed at a distance R_m from the steel core. The magnetic flux density outside the wires (r > d_c/2) is:

$$B_o(r) = \frac{\mu_0 \cdot I \cdot N_1}{2 \cdot \pi \cdot r} \tag{9}$$

The inductance outside can therefore be obtained from:

$$L_o = \frac{\psi_o}{I} = \mu_0 \cdot \int_{R_c}^{R_m} \frac{N_1^2 \cdot l \cdot dr}{2 \cdot \pi \cdot r} =$$

$$= \frac{\mu_0 \cdot N_1^2 \cdot l}{2 \cdot \pi \cdot r} \cdot \ln\left(\frac{R_m}{R_c}\right) \tag{10}$$

Inside the group of wires ($r < d_c/2$) the magnetic flux density is:

$$B_i(r) = \frac{\mu_0 \cdot I \cdot r \cdot N_1}{2 \cdot \pi \cdot R_c^2} \tag{11}$$

And the inductance inside the group of wires is given by:

$$L_i = \frac{\psi_i}{I} = \mu_0 \cdot \int_0^{R_c} \frac{N_1^2 \cdot l \cdot r^3}{2 \cdot \pi \cdot R_c^2} \cdot dr = \frac{\mu_0 \cdot N_1^2 \cdot l}{8 \cdot \pi} \tag{12}$$

Therefore the end-winding inductance per phase is:

$$L_{end} = 2 \cdot k \cdot \mu_o \cdot N_1^2 \cdot R_m \cdot \ln\left(\frac{R_m}{R_c \cdot e^{-\frac{1}{4}}}\right) \tag{13}$$

Where k is the number of LSRM sides (k = 2 double-sided, k = 1 single-sided), N_1 the number of wires per pole, $l = 2 \cdot \pi \cdot R_m$ and R_c is the equivalent radius considering the copper area (A_{Cu}):

$$R_c = \sqrt{\frac{A_{Cu}}{\pi}} = \sqrt{\frac{c_p \cdot l_p \cdot k_v}{2 \cdot \pi}} \tag{14}$$

Where k_v is the slot fill factor.
Finally the end-winding inductance per phase L_{end} is:

$$L_{end} = k \cdot N_1^2 \cdot \mu_0 \cdot (b_p + \frac{c_p}{2}) \cdot \ln\left(\frac{\sqrt{\pi} \cdot (b_p + \frac{c_p}{2})}{e^{-\frac{1}{4}} \cdot \sqrt{c_p \cdot l_p \cdot k_v}}\right) \tag{15}$$

B. End-winding inductance: 2D-FEA

End-winding inductance can be calculated using a 2D FEM axis-symmetric solver [8] by means of the model shown in Fig. 5. Each wire is considered an independent circuit.

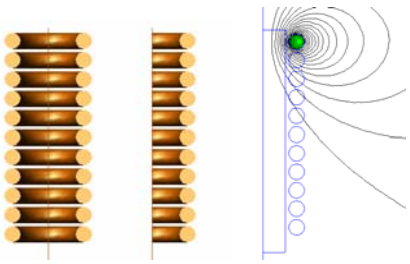

Fig. 5: Axis-symmetric FEM model for computing L_{end}.

The end-winding inductance per phase is computed using the following expression:

$$L_{end} = 2 \cdot k \cdot \sum_{i=1}^{N_1} \left(L_i + \sum_{j=1}^{N_1} M_{i,j} \right) \tag{16}$$

Where L_i is the self inductance from i-wire and M_{ij} is the mutual inductance between wires i and j obtained by:

$$L_i = \frac{1}{I_i^2} \cdot \iint J_i \cdot A \cdot dS \tag{17}$$

$$M_{i,j} = \frac{1}{I_i} \cdot \oint_j \overline{A}_j \cdot dl \tag{18}$$

Where $\overline{A}_j$ is the average magnetic potential over the surface S_j obtained by:

$$\overline{A}_j = \frac{1}{S_j} \cdot \iint_{S_j} A \cdot dS \tag{19}$$

Table I shows the results obtained analytically by means of (15) and numerically by (16).

The equation (16) can be implemented in *Lua* script [8-9] for automatically computing end-winding inductance. The code is shown in the annex.

TABLE I. – Comparison results for L_{end}

Analytically (15):	L_{end}= 1,39μH
by FEM (16):	L_{end}= 1.08μH

4. Corrected 2D FEA

The complete double-sided LSRM prototype is shown in Fig. 6 and its main dimensions are given in table II.

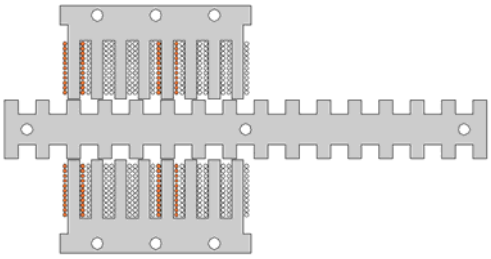

Fig. 6. 2D view of the double sided LSRM prototype

TABLE II. – LSRM prototype main dimensions

	SYMBOL	VALUE (UNITS)
Number of phases	m	4
Stator pole width	b_p	6 (mm)
Stator slot width	c_p	6 (mm)
Stator pole pitch	T_p	12 (mm)
Number of active poles per side (stator)	N_p	8
Stator pole length	l_p	30 (mm)
Translator pole width	b_s	7 (mm)
Translator slot width	c_p	9 (mm)
Translator pole pitch	T_p	16 (mm)
Number of passive poles per side (translator)	N_s	6
Translator pole length	l_s	7 (mm)
Yoke height	h_y	8 (mm)
Stack length	L_W	30 (mm)
Air gap length	g	0.5 (mm)
Stroke	PS	4 (mm)
Number of turns per pole	N_1	11
Wire diameter	d_c	2.1 (mm)

The translator moves from the aligned to the unaligned position for different excitation currents. Fig. 7 shows the flux lines obtained from 2D FEA [8]

.

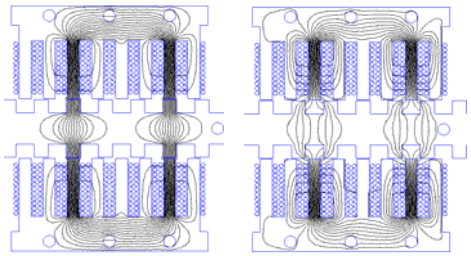

(a) (b)

Fig. 7: Flux plots from 2D FEM analysis of the LSRM a) Aligned b) Unaligned

Values obtained for L_{end} (see table II) are applied in (2) in order to correct the 2D FEM results and the magnetization curves obtained are compared for the aligned and unaligned positions (see Fig.8). There is almost no difference between the magnetization curves whether the L_{end} is obtained analytically or numerically, as can be seen in Fig. 8.

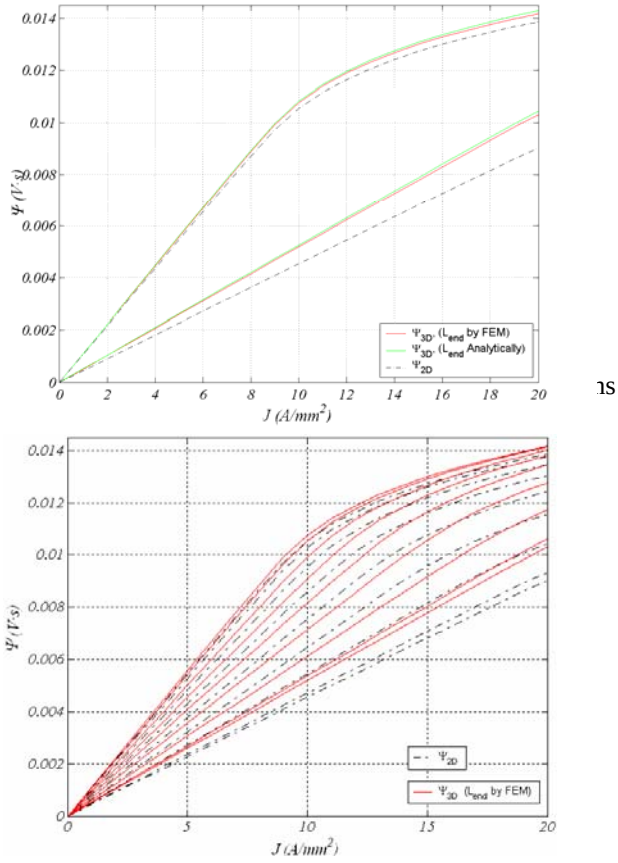

Fig. 9. Comparison of Ψ_{2D} FEM results and corrected Ψ_{3D} computed for intermediate positions

Fig. 9 shows the magnetization curves, flux linkage versus current for the different positions of the translator, obtained by 2D FEA, Ψ_{2D} and the same curves corrected by the end-effect coefficient, Ψ_{3D}.

The co-energy (W'_{3D}), knowing (Ψ_{3D}), is calculated using the well-known expression:

$$W'_{3D}(x_i, I) = \int_o^I \psi_{3D}(x, i) \cdot di \Big|_{x_i = Ctn} \quad (20)$$

Then, the propulsion force, including end effects, is obtained by:

$$F_{x,3D}(I) = \frac{\partial W'_{3D}(x, I)}{\partial x} \Big|_{I = Ctn} \quad (21)$$

The influence of end effects on the propulsion force is clearly shown in Fig. 10.

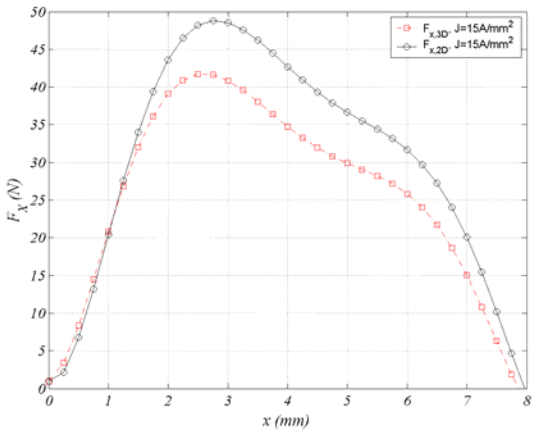

Fig. 10. 2D and 3D propulsion force

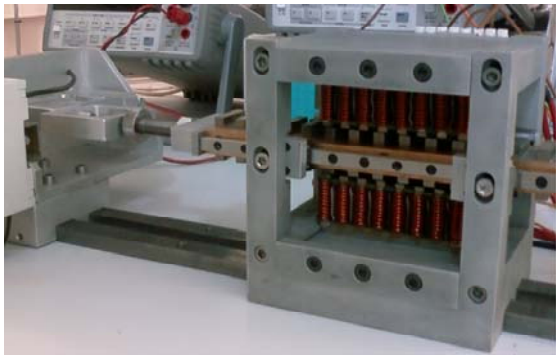

Fig. 11. View of the test setup and of the double-sided LSRM prototype

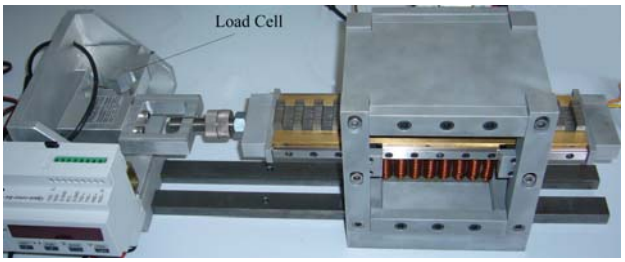

Fig. 12. View of the test setup and load cell detail

5. Experimental results

The LSRM was tested in order to evaluate the results obtained by means of the proposed procedure. A test setup was built to perform the experimental measurements (Fig.11). The flux linkage–current curves were obtained following the procedure described in [10].

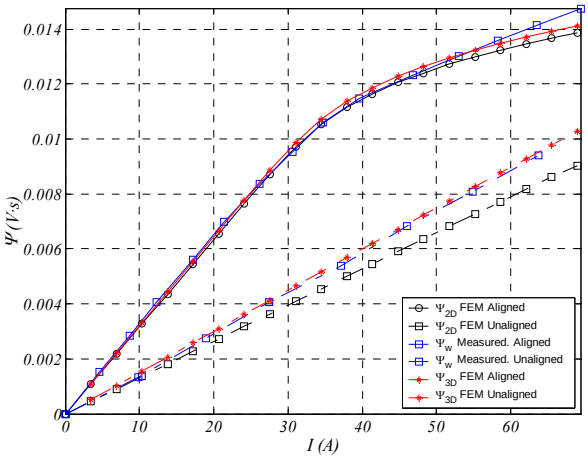

Fig. 13. Ψ_{2D}, Ψ_{3D} and measured flux linkage vs. current for aligned and unaligned position

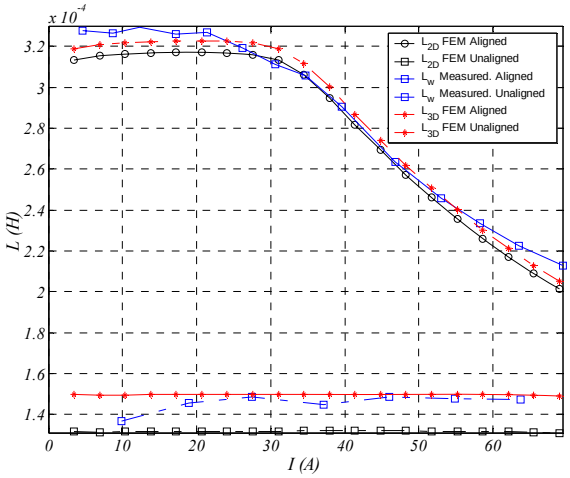

Fig. 14. L_{2D} , L_{3D} and measured inductance vs. current for aligned and unaligned position

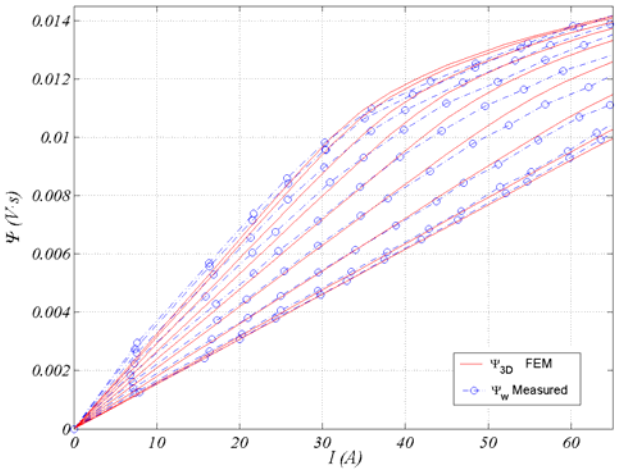

Fig. 15. Ψ_{3D} and measured flux linkage vs. current for intermediate positions ($0 \le x \le S$) and Δx=1mm

Inductances were directly obtained from the flux linkage–current curves ($L=\Psi/I$) and the propulsion force was measured directly by a load cell. The comparison between the results obtained with the proposed procedure and the experimental test of magnetization curves (Ψ_{3D} *vs.* I) and inductances (L_{3D} *vs.* I) in the aligned and unaligned positions are plotted in Fig.13 and Fig.14 respectively. Fig.15 shows the comparison between the 2D FEM results including end-effects and the experimental results for intermediate positions. The measured force versus the values derived from equation (21) can be seen in Fig.16.

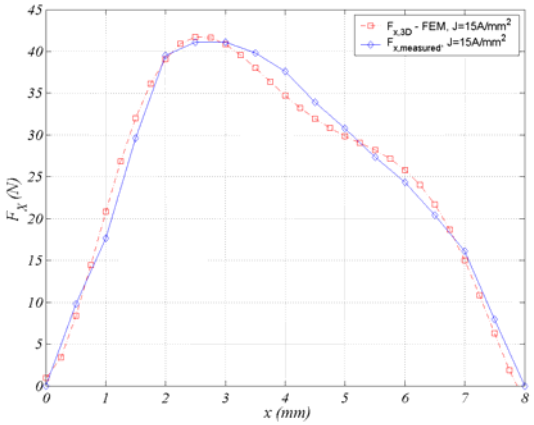

Fig. 16. 3D and measured propulsion force.

6. Conclusions

This paper studies the end effects in double-sided LSRM and proposes a procedure based on 2D FEM corrected by the inclusion of end-winding inductance and several empirical coefficients. This procedure was proven by experimental measurements in a test setup especially constructed for this purpose. The approach proposed here may be very useful in LSRM design.

Acknowledgements

This research was supported by the Spanish Ministry of Education and Science and the ERDF (DPI2006-09880).

Annex

Lua script algorithm for L_{end} computation

```
1:  k=2; J=15e6;--(MA/m^2)
2:  Lend=0; M=0; L=0; I=J*π*dc^2/4
3:  for i=1,Nl do
4:    mi_modifycircprop(i,1,I)
5:    mi_analyze(1); mi_loadsolution()
6:    for j=1,Nl do
7:     if j==i then
8:       mo_groupselectblock(j)
9:       Li=mo_blockintegral(0)/I^2
10:      L=L+Li
11:      mo_clearblock()
12:    else
13:      mo_groupselectblock(j)
14:      Si=mo_blockintegral(5)
15:      Mi=mo_blockintegral(1)/(I^2* Si)
16:      M=M+Mi
17:      mo_clearblock()
18:    end
19:   end
20:   mo_close()
21: end
22: Lend=2*k*(L+M)
```

References

[1] T.J.E Miller, “Optimal Design of Switched Reluctance Motors”. IEEE Transactions on Industrial Electronics, vol. 49, no. 1, pp. 15-27, Feb 2002

[2] A. Michaelides, C. Pollock, “Effect of End Core Flux on the Performance of the Switched Reluctance Motor” IEE Proceedings Electric Power Applications, vol. 141, no. 6, pp. 308-316, 1994.

[3] Y.Sofiane, A.Tounzi, F.Piriou, M.Liese, “Study of Head Winding Effects in a Switched Reluctance Machine”, IEEE Transactions on Magnetics, vol. 38, no. 2, pp. 989-992, March 2002.

[4] A. Matveev, V. Kuzmichev, and E. Lomonova, “A new comprehensive approach to estimation of end-effects in switched reluctance motors”, Proceedings ICEM2002, Bruges, Belgium, August 2002

[5] F. D’hulster, K. Stockman, R.J.M. Belmans “Modelling of Switched Reluctance Machines: State of the Art” International Journal of Modelling and Simulation, vol. 24, no. 4, pp. 216-223, 2004

[6] A. B. J. Reece, T. W. Preston, “Finite element Methods in Electrical Power Engineering” Oxford University Press. Oxford 2000. pp. 201-211

[7] U. Deshpande, “Two-Dimensional Finite Element Analysis of a High-Force Linear Switched Reluctance Machine Including Three-Dimensional Effects” IEEE Transactions on Industry Applications, vol. 36, no. 4, pp. 1047-1052, July/August 2000.

[8] D.C. Meeker, Finite Element Magnetics Method. Version 4.2 *FEMM4.2* .15 May 2008 (*http://femm.foster-miller.net*)

[9] Lua Reference manual version 4.0 (*http://www.lua.org*) Nov. 2000.

[10] H. Bausch, K. Kanelis, “Feedforward Torque Control of a Switched Reluctance Motor Based on Static Measurement” ETEP, vol. 7, no. 6, pp. 373-380, November/December 1997.